Received: January 3, 2024. Revised: March 16, 2024.

INASS

International Journal of
Intelligent Engineering & Systems

http://www.inass.org/

Robust Control and Energy Management in Grid-connected Photovoltaic-battery Energy Storage Systems

Salwa Naddami[1]* **Najib Ababssi[1]**

[1]*Industrial Management and Innovation Laboratory, Faculty of Science and Technology, Hassan First University Settat, Morocco*
* Corresponding author's Email: s.naddami@uhp.ac.ma

Abstract: This paper investigates the design of a robust non-linear backstepping controller for the DC-AC microgrid comprising a photovoltaic source and a battery energy storage system with grid integration, all feeding a non-linear load, to improve its power quality and dynamic stability. A unidirectional DC-DC boost converter and a bidirectional back boost converter are used on the DC side to connect the photovoltaic module and battery storage to the DC bus. The three phases of the voltage source inverter are connected to the electrical grid via an inductive filter on the AC side. The control objectives are fourfold: i) Produce the maximum power from the photovoltaic system regardless of variations in weather conditions (temperature and irradiation); ii) Keep the DC link voltage constant and close to a given reference value under various conditions to ensure a balance of power between the DC and AC sides; iii) Active power control by injecting excess power into the grid; iv) Propose an energy management strategy to optimize the energy consumption of each source: the solar source, the grid, and the battery storage. Simulation results under different operating conditions, parameter variations, and load disturbances are presented and discussed to verify the performance satisfaction of the proposed controllers. An improvement in the overall dynamic performance of the microgrid is demonstrated, with a reduction in voltage overshoot (4.8%) and settling time (5.6ms) on the DC bus, along with reduced total harmonic distortion (THD) in grid current (0.29%) when compared with the other controllers in this work: the proportional integral controller (voltage overshoot (5.8%), settling time (15.5ms); grid current THD (6.53%)) and sliding mode controller(voltage overshoot (4.6%), settling time (15ms), grid current THD (3.53%). finally, several tests have been conducted on the proposed microgrid to evaluate the controller's efficiency in maintaining power balance during irradiation distortion and non-linear load imbalance.

Keywords: Energy storage system, Buck-boost converter, Energy management, Renewable energy system, Robust control.

1. Introduction

Renewable energy sources (RES) are widely recognized for their effectiveness and resilience in reducing environmental pollution and promoting the generation of clean electrical energy. For example, Morocco has the goal to accomplish 52% of renewable energy by 2030 [1, 2]. However, due to the unpredictability of renewable energy sources, it is not possible to use them autonomously without integrating energy storage systems [3–5]. Batteries are widely used in microgrids due to their ease of implementation and availability, making them the most common energy storage technology. [6–8], as we need to store the surplus energy produced by RES and use it when production is insufficient to meet electricity demand. DC and AC converters are essential components in photovoltaic systems connected to microgrids. They serve as intermediary power supply units for storing the energy generated by the photovoltaic system [9, 10]. A unidirectional DC/DC Boost converter is included on the DC side to guarantee that the PV generator produces the maximum amount of power possible [11]; The battery storage system (BSS) is controlled by integrating a bi-directional buck/boost DC/DC

converter for charging and discharging. [12]. A three-

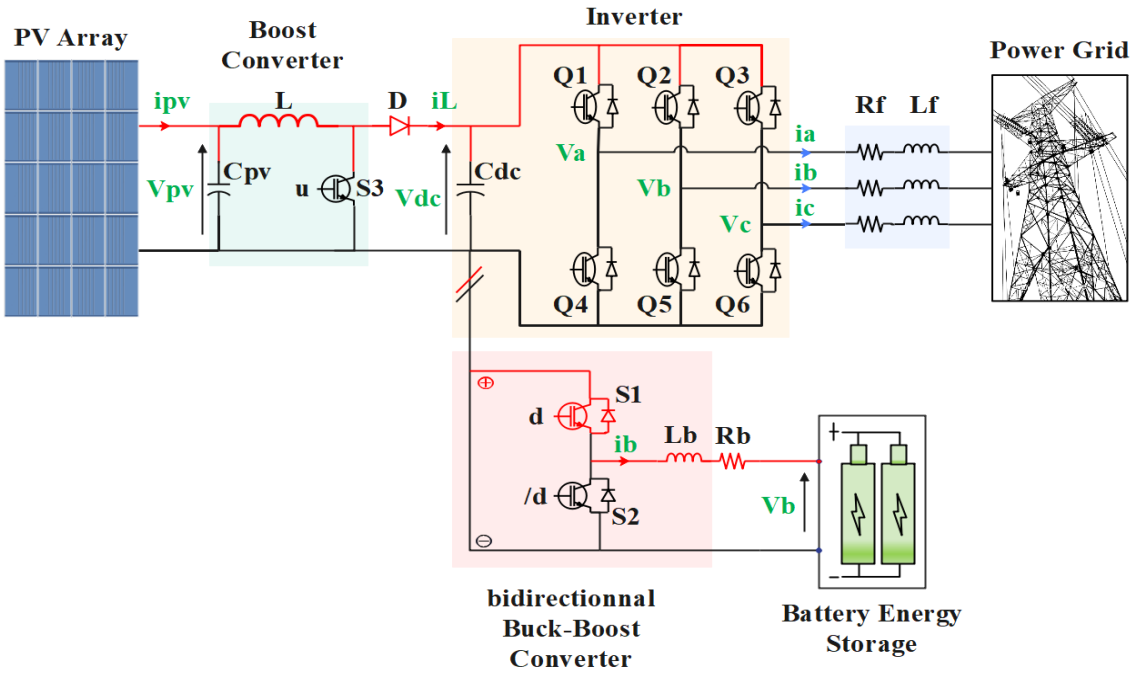

Figure. 1 Detailed structure of the proposed microgrid system

phase DC/AC voltage source inverter (VSI) is used on the AC side to ensure energy conversion and enhance the quality of the electricity [13].

To guarantee the quality and efficiency of energy transfer, the operation of DC/AC microgrids requires complex energy control and management techniques. In DC microgrids, DC bus voltage stability is crucial [14], making it one of the principal objectives. Numerous linear control techniques have been proposed [15, 16] to enhance DC bus voltage stability. However, the proposed models ignore the non-linear nature of DC-DC converters, and their operation is limited to a small region. However, DC microgrids encounter dynamic operating points due to the intermittency of renewable energy sources. Thus, linear controllers are inadequate to handle fast transients, such as a sudden change in load demands or a sudden generation loss. In [17, 18], a nonlinear sliding-mode controller is utilized to regulate the DC bus voltage and control the amount of power injected into the grid to ensure the stability of a three-phase grid-connected PV system. Nevertheless, the controller exhibits reduced sensitivity to external disturbances and encounters a chattering phenomenon.

In this paper, a robust backstepping control for grid-connected PV systems with battery energy storage is advanced to realize the following objectives:1) produce maximum power for the PV system. 2) Optimize the energy storage and buck-boost converter regulation.3) Regulate the DC bus for power balance regardless of load changes, the unpredictability of renewable sources, and external disturbances.4) Guarantee the overall stability of the microgrid despite variations in photovoltaic power and non-linear load conditions. The system topology, including PV, battery, boost converter, buck-boost converter, and voltage source inverter, is simulated and analysed in MATLAB/Simulink. The proposed control is shown to have good tracking, with reduced overshoot, chattering, and settling time.

This document is structured as below: Part 2 describes the mathematical modelling of the DC/DC and DC/AC components of the microgrid. Part 3 explains the control strategy of the power converter. Part 4 describes the formulation of the power management algorithm. Part 5 presents the simulation results of the proposed control method. Finally, part 6 summarizes the paper.

2. The design of the proposed AC/DC microgrid system and the dynamic modelling of its components

This section provides an analysis of system resources with modelling of their DC-DC and DC-AC power converters, including mathematical expressions for resource output voltages and power converter state-space models.

The system includes a PV module (100kw) and a lithium-ion battery connected to the common DC bus through a unidirectional boost converter and a

bidirectional buck boost converter as shown in Fig. 1. The converter is linked to the AC microgrid through a three-phase voltage-source inverter and an inductive filter, ultimately connected to the PCC. All these components supply power to a non-linear load.

2.1 Modeling of solar PV unit with unidirectional boost converter

2.1.1. PV array modeling

The photovoltaic module comprises solar cells linked in series and parallel. Series connection ensures the necessary output voltage, while parallel connection boosts the output current. Various solar cell types are employed in photovoltaic systems, including the single diode and the double diode. The single diode is the most widely used circuit model, extensively studied in numerous research [19].

The mathematical equation describing the current-voltage characteristics of the PV module is as [20]:

$$I_{pv}=I_{ph}-I_s\left(e^{\frac{V_{pv}+R_sI_{pv}}{aV_t}}-1\right)-\frac{V_{pv}+R_sI_{pv}}{R_{sh}} \quad (1)$$

Where: I_{ph} , I_s , and I_{pv} represent the current generated by incident solar irradiation, diode reverse leakage current, and terminal current of the PV module. Vpv and Vt denote the thermal voltage of the PV module, which is calculated as Vt=kT/q; where q represents the charge of an electron (1.6 x 10-19 C); K is Boltzmann's constant (1.380 × 10−23 J/K); T represents the module working temperature. Rp and Rs correspond to the Shunt and Series resistances of the PV module, respectively. Finally, a signifies the ideality factor.

2.1.2. Model of DC-DC boost converter

Boost converters are a type of switching DC-DC converter that step effectively step up the input voltage to a higher output voltage. This DC-DC boost converter is often utilized to match the PV generator with the DC bus while ensuring that the PV generator operates at its maximum power point (MPP) through the duty cycle (u). The following dynamic equations can be formed by successively applying the Kirchhoff laws with u = 1 and u = 0 to the boost converter circuit shown in Fig. 1. [21]

$$\frac{dVpv}{dt}=\frac{1}{Cpv}I_{pv}-\frac{1}{Cpv}i_L \quad (2)$$

$$\frac{diL}{dt}=\frac{1}{L}V_{pv}-\frac{1}{L}(1-u)V_{dc} \quad (3)$$

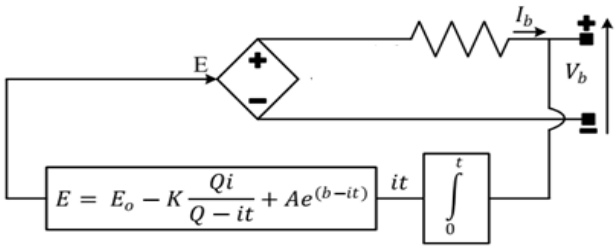

Figure. 2 Dynamic model of lithium battery

2.2 Modeling of battery energy storage system with a bidirectional buck-boost converter

Various energy storage technologies are available, each with distinct characteristics such as the storage medium used, response time, power density, energy density, lifetime, and efficiency [22,23]. The main objective of this study is to examine the applications of BES, which is one of the fast-response energy storage technologies.

2.2.1. Battery energy storage modeling

Battery energy storage is widely recognized as the oldest and most established storage system, where electrical energy is stored in the form of chemical energy [6]. A battery energy storage (BES) system comprises multiple cells connected in series and parallel. Each cell consists of a cathode and an anode, separated by an electrolyte. As the battery charges or discharges, electrochemical reactions occur within the individual cells, allowing the battery to either absorb or supply energy from/to the grid.

The equivalent circuit diagram of a battery can be seen as a simple electrical model of a battery cell. It consists of the electromotive force E in series with the internal resistance indices R_b of the battery. Applying Kirchhoff's law, we obtain the modeling of this battery where the voltage source E is described in Fig. 2. [24]

$$V_b=E-R_bi_b \quad (4)$$

$$E=E_0-K\frac{Q_i}{Q-\int i_b dt}+Ae^{B\int i_b dt} \quad (5)$$

E_0 represents the constant battery voltage. E denotes the open-circuit voltage. Q is the battery capacity, K is the polarization voltage, A is the amplitude of the exponential zone, I represent the current, idt is the actual battery charge, and b is the inverse of the time constant of the exponential zone.

2.2.2. Bidirectional buck-boost converter modelling

The battery is connected to the DC bus via the buck-boost converter, which consists of the inductor

L_b with its equivalent series resistance R_b and two IGBT switches S1 and S2 as shown in Fig. 1.

A bidirectional DC-DC converter is used with the BESS to maintain the balance between supply and demand in the DC microgrid by controlling the charging and discharging processes by applying a binary signal to the switch's gates u_b {0,1}. According to the SoC and load demand, it can work in either buck or boost mode When the battery is operating in discharge mode, the DC-DC converter is in boost mode ($I_{bref} > 0$) and supplies power to the DC bus. At this moment, S2 is switched off and S1 is ON. When the battery works in the charging mode, the energy is transferred from the DC bus to the battery side. At this point, the DC-DC converter is in the buck mode ($I_{bref} < 0$), where S1 is turned off and S2 is ON.

we can get the whole mathematical model of the bidirectional DC-DC converter expressed as:

$$\frac{dIb}{dt} = \frac{1}{Lb}(V_b - R_b I_b - u_b V_{dc}) \tag{6}$$

$$\frac{dVdc}{dt} = \frac{1}{C_{dc}}(u_b I_b - I_{dc}) \tag{7}$$

Where Ib denotes the current output of the converter, VB represents the voltage at the battery terminal, Lb signifies the inductance of the converter, R_b represents its internal resistance, and u_b denotes the input converter command received by the controller.

2.3 Modelling of voltage source inverter and filter

The three-phase inverter is used to transform the voltage from DC to three-phase AC voltage [25]. The differential equations for each phase model the AC side of the conversion system. Considering inductor unsaturation and disregarding iron and copper losses due to skin effects, the filter equation L_f becomes:

$$V_a = Ri_a + L_f \frac{di_a}{dt} + e_a \tag{8}$$

$$V_b = Ri_b + L_f \frac{di_b}{dt} + e_b \tag{9}$$

$$V_c = Ri_c + L_f \frac{di_c}{dt} + e_c \tag{10}$$

Using vector notation, these equations can be expressed in the frame of the d-q rotation as follows:

$$V_d = RI_d + L_f \frac{dI_d}{dt} + L_f w I_q + E_d \tag{11}$$

$$V_q = RI_q + L_f \frac{dI_q}{dt} - L_f w I_d + E_q \tag{12}$$

According to the following equation, the converter's DC side is represented:

$$C_{dc} \frac{dVdc}{dt} = i_L - i_{dc} \tag{13}$$

The DC link's current can be determined by the power on the AC side. Where: $i_{dc} = \frac{2}{3}\frac{E_d}{V_{dc}} I_d$

Since it is necessary for the power on the DC side to be equal to that on the AC side of the converter, the principle of power balance can be reformulated as follows, assuming that the converter suffers no power loss.

$$P_{dc} = P_g \ , \ V_{dc} i_{dc} = \frac{2}{3} E_d I_d \tag{14}$$

$$\frac{dVdc}{dt} = \frac{1}{C_{dc}}(i_L - (\frac{3}{2}) \frac{E_d}{V_{dc}} I_d) \tag{15}$$

Thus, the following equation can be utilized to represent the state space in d-q coordinates for the VSI, which is connected to the electrical grid via the L filter.

$$\frac{dVdc}{dt} = \frac{1}{C_{dc}}\left(i_L - \frac{3}{2V_{dc}} E_d I_d\right) \tag{16}$$

$$\frac{dI_d}{dt} = wI_q - \frac{R}{Lf} I_d - \frac{E_d}{Lf} + \frac{Vd}{Lf} \tag{17}$$

$$\frac{dI_q}{dt} = -wI_d - \frac{R}{Lf} I_q - \frac{E_q}{Lf} + \frac{V_q}{L_f} \tag{18}$$

3. Proposed controller design

This section presents the design of the proposed non-linear controller for grid-connected photovoltaic systems with energy storage batteries, as shown in Fig. 1. The control circuit is intended to accomplish three main objectives.

Firstly, it aims to ensure that the photovoltaic module generates the maximum available power. Secondly, it maintains the intermediate circuit voltage at a fixed value to ensure power balance in the system, and finally manages energy by storing and releasing excess energy. Six control loops were used to achieve these objectives. Cascade current and voltage control loops on the PV side, intermediate circuit voltage control loops, active and reactive power control loops on the inverter side, and battery current on the storage side. The system is divided into sub-systems. The stability of each subsystem is

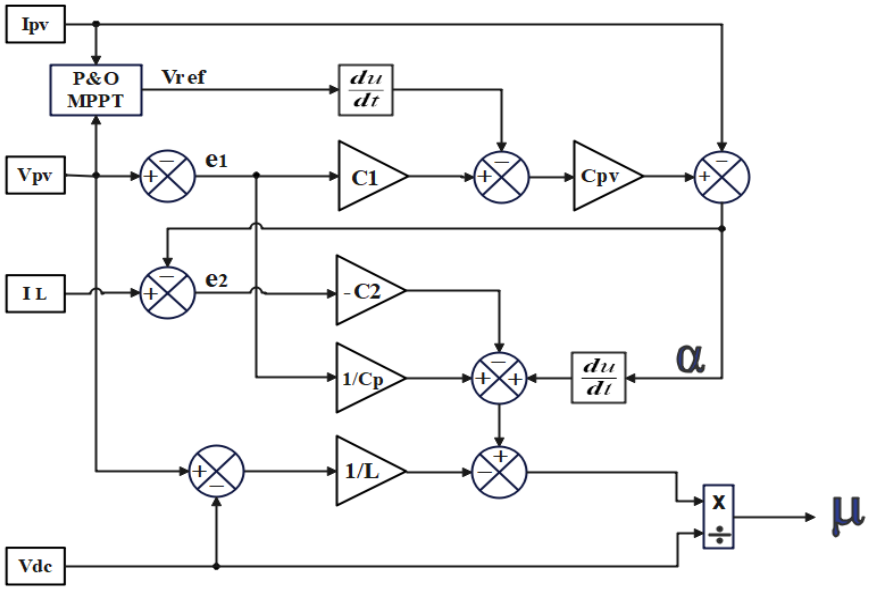

Figure. 3 Controller Bloc for boost MPPT

obtained using the Lyapunov stability approach at different stages of the design process.

3.1 Boost converter control design

The primary concept of the nonlinear backstepping controller (BSC) is to iteratively create a control law. This approach aims to follow the maximum power point of a photovoltaic system (PV) and to adjust the output voltage of the PV generator according to the reference voltage produced by the widely used MPPT algorithm perturbation and observation (P&O), This is achieved by controlling the duty cycle μ of the boost power converter.

Consequently, the boost converter control input is achieved using the dynamic model described by the Eqs. (2) and (3)

The input command is expressed as follows using the backstepping technique [26], as in Fig. 3.

$$u=\frac{L}{V_{dc}}[-C_2\mathcal{E}_2+\frac{1}{C_p}\mathcal{E}_1-\frac{1}{L}(V_p-V_{dc})+\dot{\alpha_1}] \quad (19)$$

with: $\mathcal{E}_1=V_{pv}-V_{ref}$; $\alpha_1=I_{pv}+C_{pv}(C_1\mathcal{E}_1-\dot{V}_{ref})$; and $\mathcal{E}_2=I_L-\alpha_1$

where C1 et C2 are the positive performance parameter of the backstepping controller.

3.2 Bidirectional buck boost converter control design

The dynamical model outlined by Eq. (6) is used to design the switching control input for the bidirectional buck-boost converter, see Fig. 4. To design the controller, the objective now is to find a suitable u_b such that e_b is 0.

Step 1

The tracking error between the battery current and its reference value is defined as follows:

$$e_b=I_b-I_{bref} \quad (20)$$

The derivative of the tracking error with respect to time can be expressed as follows:

$$\dot{e_b}=\frac{1}{L_b}(V_b-R_bI_b-u_bV_{dc})-\dot{I_{bref}} \quad (21)$$

Lyapunov candidate function and its time derivative

$$V_b(e_b)=\frac{1}{2}e_b^2 \quad (22)$$

$$\dot{V_b}(e_b)=e_b\dot{e_b}=e_b[\frac{1}{L_b}(V_b-R_bI_b-u_bV_{dc})-\dot{I_{bref}}] \quad (23)$$

The command u_b is chosen to obtain the following expression:

$$\frac{1}{L_b}(V_b-R_bI_b-u_bV_{dc})-\dot{I_{bref}}=-K_be_b \quad (24)$$

The non-linear backstepping control law can be deduced as follows.

$$u_b=\frac{1}{V_{dc}}[V_b-R_bI_b+L_b(K_be_b-\dot{I_{bref}})] \quad (25)$$

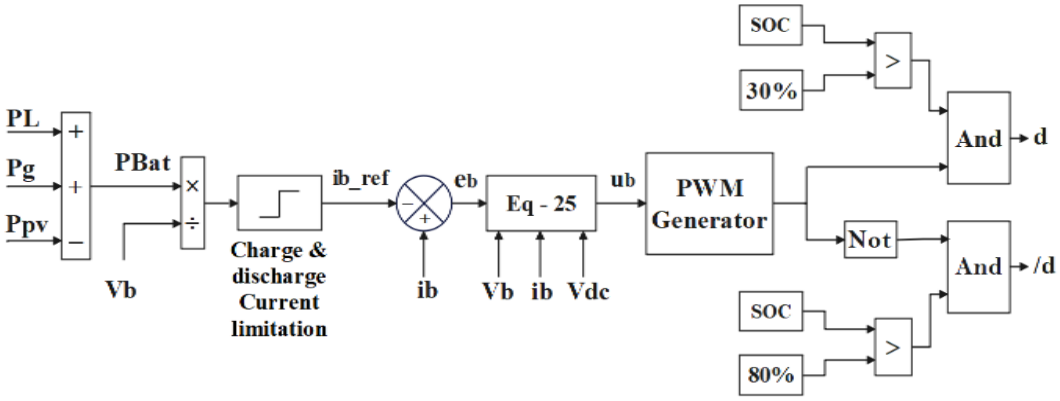

Figure. 4 Controller bloc for buck-boost converter

3.3 Voltage source inverter control design

To ensure a smooth transfer of surplus power from the photovoltaic panel to the grid, the voltage source inverter is controlled by cascading the control of the DC link voltage and grid currents. This enables operation with a unity power factor.

In the d-q synchronous reference frame (Eq=0), the mathematical model simplifies the injected powers, allowing active and reactive powers to be controlled by V_{dc} , Id and Iq respectively:

$$P = \frac{3}{2}(E_d I_d + E_q I_q) = \frac{3}{2}E_d I_d \quad (26)$$

$$Q = \frac{3}{2}(E_d I_q - E_q I_d) = -\frac{3}{2}E_d I_q \quad (27)$$

The control block diagram using the backstepping strategy proposed in this article is shown in Figure 6. According to the mathematical equation in Eqs. (16-18), which models the dynamics of the converter, the following elements are considered: Voltages Vd and Vq are input commands, while the bus voltage DC and currents id and iq are regarded as outputs. The tracking errors of the the DC bus voltage, dq current axis are identified as the difference between the actual value of Vdc, id and iq and their references.

Step 1: DC link voltage control

The main purpose of the controller in this subsystem is to regulate active power while maintaining a constant DC link voltage at a reference value, regardless of any system disturbances. However, the reference value of the grid current Id depends on the total amount of active power provided to the grid, which is also related to the voltage of the DC link reference value.

In the first step, the DC link voltage is stabilized by introducing the tracking error below:

$$\mathcal{E}_3 = V_{dc} - V_{dcref} \quad (28)$$

Time-derivative of the of the error dynamic (28) is defined as follows:

$$\dot{\mathcal{E}}_3 = \frac{1}{C_{dc}}\left(i_L - \frac{3}{2V_{dc}}E_d I_d\right) \quad (29)$$

Using Eqs. (28) and (29) Lyapunov function and its time derivative are rewritten as:

$$V_3 = \frac{1}{2}\mathcal{E}_3^2, \dot{V}_3 = \mathcal{E}_3\dot{\mathcal{E}}_3 = \mathcal{E}_3\left(\frac{i_L}{C_{dc}} - \frac{3}{2V_{dc}}E_d I_d\right) \quad (30)$$

Tracking error $\mathcal{E}_3$ is stabilized at zero by considering I_d as a virtual control input. It must be chosen in such a way that V_3 becomes a negative definite function. If the virtual value of Id is α_2 , it can be chosen as follows.

$$\alpha_2 = (I_d)_d \ , \ \alpha_2 = \frac{2C_{dc}V_{dc}}{3E_d}\left(C_3\mathcal{E}_3 + \frac{i_L}{C_{dc}}\right) \quad (31)$$

The choice of the virtual control input α_2 guarantees that Eq. (30) produces a negative semidefinite function, as demonstrated in the following equation: $\dot{V}_3 = -C_3.\mathcal{E}_3^2$

Step 2: active power control

The virtual control α_2 is not equal to the d-axis current in the first step, there is an error between them .to correct this error, another tracking error for the d-axis current and its time derivative as shown below:

$$\mathcal{E}_4 = I_d - \alpha_2 \ , \ \dot{\mathcal{E}}_4 = wI_q - \frac{R}{L_f}I_d - \frac{E_d}{Lf} + \frac{Vd}{Lf} - \dot{\alpha}_2 \quad (32)$$

The Lyapunov candidate function and the time derivative can be defined as:

$$V_4 = \frac{1}{2}\mathcal{E}_4^2 + V_3 \ , \ \dot{V}_4 = \mathcal{E}_4\dot{\mathcal{E}}_4 + \dot{V}_3 \quad (33)$$

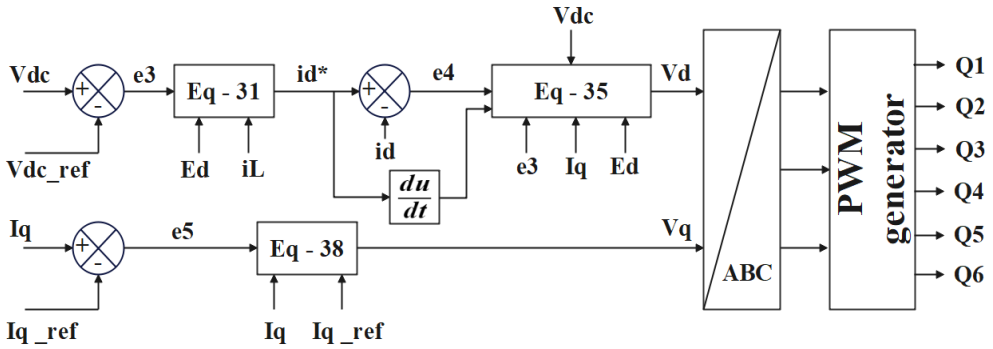

Figure. 5 Controller bloc diagram for VSI

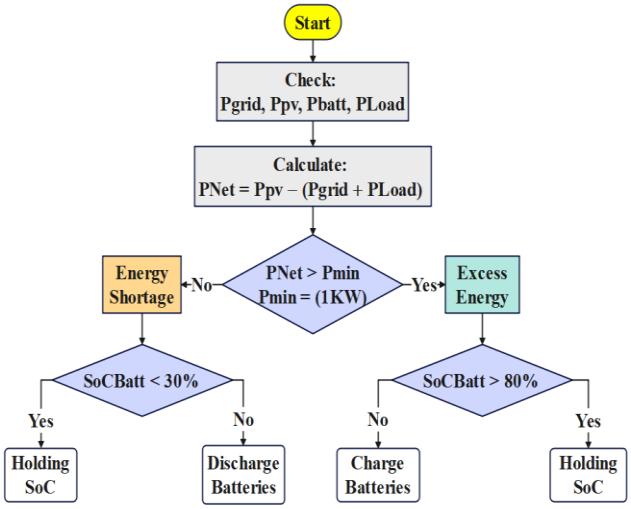

Figure. 6 Flowchart of energy management

By substituting Eqs. (30) and (32) into Eq. (33), the time derivative of the LCF can be expressed as follows:

$$\dot{V}_4 = -C_3\mathcal{E}_3^2 + \mathcal{E}_4\left[-\frac{3}{2V_{dc}}E_d + wI_q - \frac{R}{Lf}I_d - \frac{E_d}{Lf} + \frac{Vd}{Lf}-\dot{\alpha_2}\right] \quad (34)$$

For the stability purposes, $\dot{V}_4$ should be negative, so: $\dot{V}_4 = -C_3\mathcal{E}_3^2 - C_4\mathcal{E}_4^2$

The V_d control law can be designed as follows to stabilize the tracking error dynamics of V_{dc} and the 1d-axis current.

$$V_d = L_f\left[-C_4\mathcal{E}_4 + \frac{3}{2V_{dc}}E_d - w\,I_q + \frac{R}{Lf}\,I_d + \dot{\alpha_2}\right] \quad (35)$$

Step 3: reactive power control

The desired reactive power can be expressed as follows: $Q_{ref} = -\frac{3}{2}E_d . I_{qref}$

The inverter should supply the required reactive power. As a result, the tracking error and its derivative for the q-axis current using the equation (18) can be written as:

$$\mathcal{E}_5 = I_q - I_{qref},\ \dot{\mathcal{E}}_5 = -wI_d - \frac{R}{Lf}I_q - \frac{E_q}{Lf} + \frac{V_q}{L_f} - \dot{I_{qref}} \quad (36)$$

The time derivative of the Lyapunov candidate function corresponding to $\mathcal{E}_5$ is as follows:

$$\dot{V}_5 = \mathcal{E}_5\left[-wI_d - \frac{R}{Lf}I_q - \frac{E_q}{Lf} + \frac{V_q}{L_f} - \dot{I}_{qref}\right] \quad (37)$$

$\dot{V}_5$ should be negative as follows to ensure the stability of this subsystem, thus: $\dot{V}_5 = -C_5\mathcal{E}_5^2$, and the expression of the effective control law, is given by:

$$V_q = L_f\left[wI_d + \frac{R}{Lf}I_q + \frac{E_q}{Lf} + \dot{I_{qref}} - C_5\mathcal{E}_5\right] \quad (38)$$

The control laws Vd and Vq are converted into three modulation signals (Va, Vb, and Vc) using inverse DQ/ABC transformation. These modulation signals are then utilized to produce gate signals (Q1, Q2, Q3, Q4, Q5, Q6) through pulse-width modulation (PWM), as illustrated in Fig. 5.

4. Energy management strategy

Energy storage management systems are defined as structured processes for managing energy quantities according to consumer demand. In this way, they are used to increase overall system efficiency. The selection of appropriate energy management strategies depends on the type of energy system and its components. The proposed connected PV system with storage, battery charge, and discharge management is based on the power difference between the PV system and the load on the one hand while monitoring the state of charge on the other. The flowchart is shown in Fig. 6:

Table 1. Parameters of the solar PV unit

Component	Values
Vmp: Voltage at Max Power (V)	29
Imp: Current at Max Power (A)	7.35
Voc: Open Circuit Voltage (V)	36.3
Isc: Short Circuit Current (A)	7.84

Table 2. Parameters of DC-DC boost converter

Components	Values
Maximum output power, Ppv (KW)	100
Inductance of boost converter (mH)	1.45e-3
Input capacitance of converter (µF)	1000
Resistance of converter (Ohm)	1e-3
Fsw (Boost switching frequency) (Hz)	5e3

Table 3. Parameters of battery energy storage system

Components	Values
Battery type	L-Ion
Maximal Power of batteries charge (KWh)	36
Rated capacity, Qb (Ah)	100
Nominal voltage of the BESS, Vb	360
Resistance of buck boost converter Rb	1e-3
Inductance of buck boost converter Lb (mH)	13e-3
Fs (buck-Boost switching frequency) Hz	5e3

Table 4. Parameters of bus DC

DC bus Capacitor Cdc (µF)	3227
DC bus nominal voltage, (V)	600

Table 5. Parameters of ac microgrid

Ac_load (load active power) (KW)	**15 - 65**
Filter inductor, Lf (mH)	3.5
Fpwm (inverter PWM frequency) (Hz)	5e3

Table 6. backstepping controller gains values

Boost Backstepping controller	
k1	100
k2	1e6
Buck boost backstepping controller	
Kb	1e5
Inverter Backstepping controller	
c1,	1e5
c2,	5e5
c3	2e7

5. Simulation result

A simulation model was developed using MATLAB/Simulink to validate the proposed grid-connected photovoltaic system with electric energy storage on lithium batteries.

all the values of the principal components used in our PV system and controllers are mentioned in the Tables 1-6.

Several scenarios are considered to observe the behavior of controllers designed to manage the energy exchange between the photovoltaic plant, the electrical network, the storage unit, and the load. Therefore, the proposed microgrid was simulated under steps with varying loads. Solar irradiation in the solar photovoltaic unit depicted in Fig. 7 is being considered for evaluating the performance of the proposed controller. Fig. 8 illustrates how the battery is charged and discharged by increasing and decreasing the state of charge. The different cases of power flow are presented as follows and illustrated in Fig. 9. To facilitate understanding, Table 7 provides an overview of the power flow in Fig. 9.

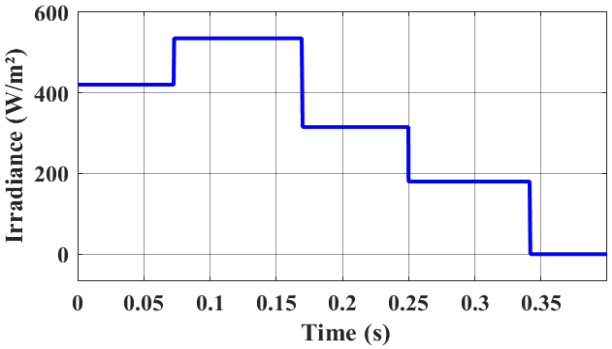

Figure. 7 Solar irradiation profile.

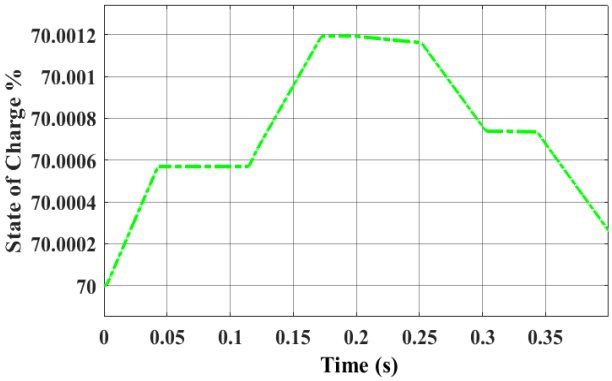

Figure. 8 Battery state of charge

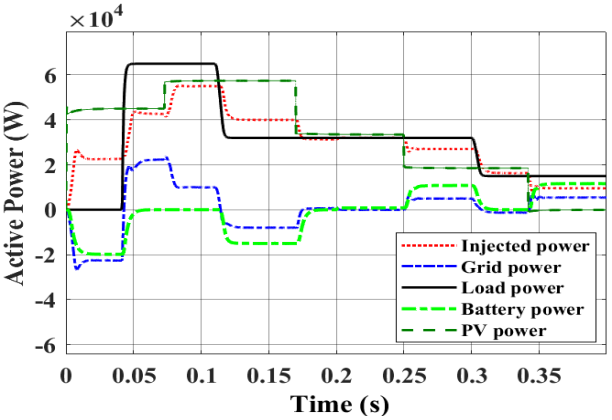

Figure. 9 Power flow at the different cases of the proposed microgrid using a backstepping controller

Table 7. Power flow of figure 9

Power Flow (KW)	Time Intervals (s)					
	0 to 0.042	After 0.042	After 0.105	After 0.18	After 0.25	After 0.35
PV	46.2	46.2 - 57	57	33	22	0
Load	0	65	32	32.3	32.3	16
Battery	19.7	0	20	0	10.1	15.6
Grid	26	20 - 8	3.7	0	0	0

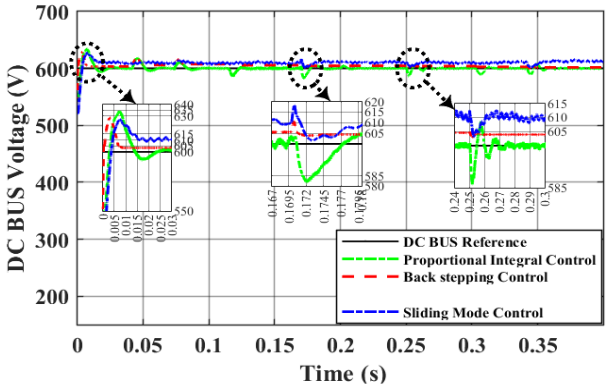

Figure. 10 Tracking performance of the DC bus voltage under change of generated power and load demand

Table 8. Analysis of DC bus voltage in quantitative form

	Transient Time (s)					
	0		0.17		0.25	
	Overshoot %	Settling time (ms)	Overshoot %	Settling time (ms)	Overshoot %	Settling time (ms)
Back stepping	4.8	5.6	1.6	< 1	1	<1
Sliding Mode	4.6	15	3	1	2	4
PI	5.8	15.5	– 3	4	2.4	10

Case 1: In case of no-load, the PV system provides energy to charge batteries whose state of charge is below the minimum threshold of 30 %, in our system, and injects the rest of the generated energy into the electricity grid. Initially, between t=0 s and t=0.042 s, the electrical consumption of the load is zero. The approximately photovoltaic power (46.2 kW) is distributed between the battery storage system (19.7 kW) and the nearby reception network (26 kW), the difference represents the filter loss to maintain the voltage of the constant DC bus (0.5 kW)

Case 2: (The load is supplied by the network and the PV system, the battery is inactive) From t = 0.043 to t = 0.105 s, the power required from the load is significantly higher than the power delivered by the power system (65 KW). The power plant is approximately (46.2 - 57 KW) corresponding to the new irradiation amplitude (440-530 W/m2), the battery has a reduced SOC so it cannot generate energy. As a result, the grid will supply the load with the lack of electricity generated by the photovoltaic battery system.

Case 3: Between t = 0.105 s and 0.180 s, the PV system continues to generate power (57 kW). Following the decrease in non-linear load power demand to (32 kW), the PV remains in constant production, divided between battery recharging (20 kW), public grid injection (3.7 KW), and load supply.

Case 4: (Load supplied by PV system, battery, and grid inactive) From t = 0.18 s to 0.25 s, the PV system displays reduced power at (33 kW) corresponding to an irradiance of 310 W/m2), the non-linear load now consumes (32.3 KW), and the grid does not supply the load and the battery remains charged. They can therefore be completely disconnected from the system.

Case 5: The state of charge has now reached its maximum value (80%) in the proposed system. From t = 0.25 s to t = 0.305 s, Load power remains constant at (32.3 kW) and the power of the photovoltaic system decreases to almost (22 kW) after the solar irradiation decreases. In this case, the non-linear load is powered by two energy sources: a photovoltaic system (22 kW), and batteries (10.1 kW).

Case 6: Finally, between t = 0.35 s and t = 0.4 s, the load drops almost to (16 kW). The battery delivers full power at load (15.6 kW), which corresponds to the battery's rated capacity given the limitation of the current delivered at load to a value of 40 A, slightly lower than the battery's rated discharge current selected in the proposed system. The photovoltaic storage system and the power plant emit no energy (0 kW) to ensure the balance between the energy generated by the photovoltaic system, grid, storage system and the load demand.

Fig. 10 shows the DC bus voltage control performance of the proposed controller in contrast to the PI and Sliding mode controls, regarding percentage overshoot and settling time across different operating modes. According to this figure and table 8, overshoot at transient 2 for the proposed control is approximately 1.6%, indicating that the

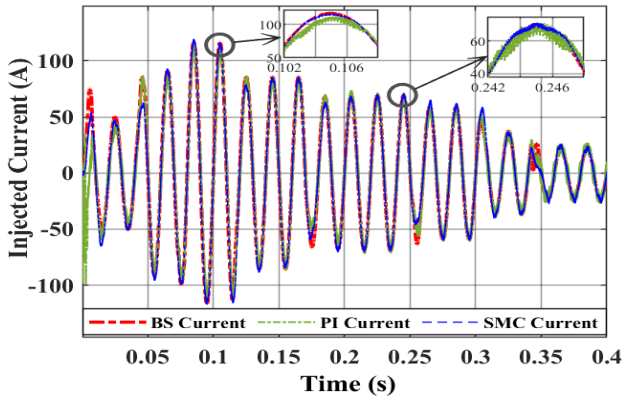

Figure. 11 grid current of phase A under irradiance variations and change of load demand

Table 9. THD values of the existing and proposed controllers

	PI	Sliding Mode	Proposed Back-Stepping
Fundamental (50 Hz)	83.16 A	85.1 A	85.79 A
THD (%)	6.53	3.53	0.29

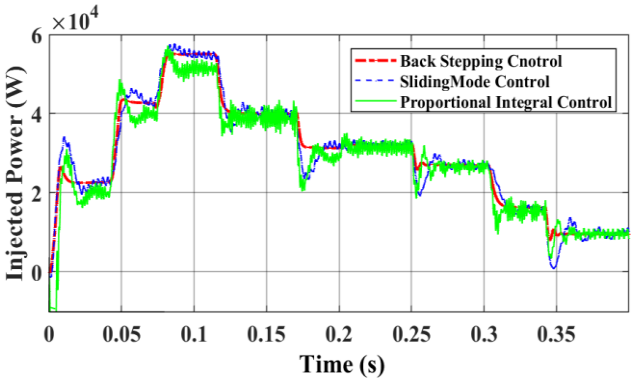

Figure. 12 Active powers injected into the grid with variation in generated power and variation in load demand

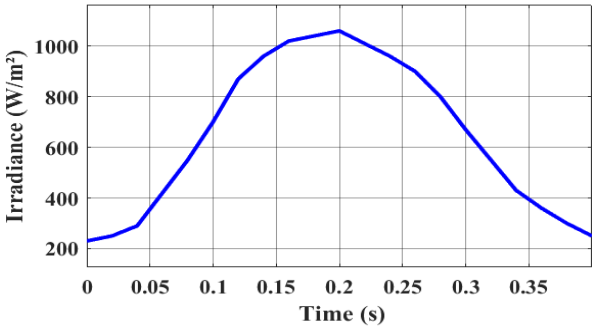

Figure. 13 Variation profile of actual irradiance

output voltage is kept below +2% of the reference voltage and has fewer exceeds. and reduced settling times of less than 1ms for the same transient.

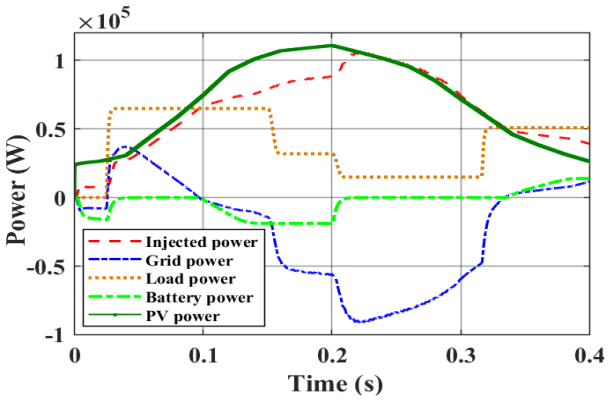

Figure. 14 Power flow (Pv power, battery power, load power and grid power) under a real irradiation variation curve

Fig. 11 shows the current of the grid under variation of the generated power and change of load demand, when using the conventional PI controller, the sliding mode controller and the proposed backstepping controller. In comparison, it is clear that the grid current of the proposed control has lower harmonics and current overshoots.

Table 9 displays the FFT analysis of grid current, indicating a THD value of 0.29% with the backstepping controller. In comparison, the grid current THD is around 6.53% and 3.53% with the proportional-integral controller and sliding mode controller, respectively, under identical conditions.

These results clearly show that the quality of the grid current with the proposed backstepping control method is significantly improved and its THD is reduced from 6.53% and 3.53% to 0.29%.

The active power injected into the grid varies according to different operating scenarios, as shown in Fig. 12. We observe that its magnitude changes in each of the previous case studies (generated power; load demand; charge battery), utilizing existing and proposed controllers. However, this figure indicates that using a PI controller and a sliding-mode controller gave satisfactory results, but with lower performance (increased fluctuations and overshoots) compared to a backstepping controller.

In this case study, the actual irradiation curve profile is considered to assess the performance and efficiency of the proposed microgrid system, as depicted in Fig. 13. Fig. 14 illustrates a scenario where energy flow is exchanged among all system components: the photovoltaic system, the battery, the load, and the power grid.

6. Conclusion

In this paper, we propose developing a non-linear backstepping controller for the different components of the microgrid-connected photovoltaic system. The

goal is to regulate the voltage of the DC link voltage loop, the active and reactive loops, the MPPT loop, and the battery current loop. We perform a stability analysis using a composite Lyapunov function to ensure the overall stability of the AC-DC microgrid. This paper also includes multiple case studies to assess the efficiency of the suggested controller in terms of maintaining power balance amidst changes in irradiation and imbalances in non-linear loads. Simulation results confirm that the controller optimizes power flow by ensuring a good balance between the different parts of the microgrid, i.e., solar PV, BESS, grid, and non-linear load, while keeping DC bus voltage levels within specified boundaries. Based on the simulation results and numerical comparison, it can be inferred that all three controllers can meet the control objective. Nevertheless, concerning dynamic stability (settling time and overshoot) and current quality across various conditions, the suggested controller outperforms the PI and Sliding Mode controllers.

Conflicts of interest

The authors declare no conflict of interest.

Author contributions

Salwa Naddami is the paper's correspondent author. She helped develop control strategies, created the proposed control of the system in MATLAB/SIULINK, and She coordinated the preparation of this work. Najib Ababssi was involved in the analysis of the power flow in the system and managed paper organization.

References

[1] M. Boulakhbar, B. Lebrouhi, T. Kousksou, S. Smouh, and A. Jamil, "Towards a large-scale integration of renewable energies in Morocco", *Journal of Energy Storage*, Vol. 32, p. 101806, 2020.

[2] S. Sahbani, H. Mahmoudi, A. Hasnaoui, and M. Kchikach, "Development Prospect of Smart Grid in Morocco", *Procedia Computer Science*, Vol. 83, pp. 1313–1320, 2016.

[3] A. N. Abdalla, M. S. Nazir, and H. Tao, "Integration of energy storage system and renewable energy sources based on artificial intelligence: An overview", *Journal of Energy Storage*, Vol. 40, p. 102811, 2021.

[4] O. Bolufawi, "Renewable Energy Integration with Energy Storage Systems and Safety", In: *Proc. of Special Topics in Renewable Energy Systems*, pp. 39–50, 2018.

[5] W. Wang, B. Yuan, Q. Sun, and R. Wennersten, "Application of energy storage in integrated energy systems — A solution to fluctuation and uncertainty of renewable energy", *Journal of Energy Storage*, Vol. 52, p. 104812, 2022.

[6] M. Moncecchi, C. Brivio, S. Mandelli, and M. Merlo, "Battery Energy Storage Systems in Microgrids: Modeling and Design Criteria", *Energies*, Vol. 13, No. 8, p. 2006, 2020.

[7] A. Bakeer, A. Chub, Y. Shen, and A. Sangwongwanich, "Reliability analysis of battery energy storage system for various stationary applications", *Journal of Energy Storage*, Vol. 50, p. 104217, 2022.

[8] K. C. Divya and J. Østergaard, "Battery energy storage technology for power systems—An overview", *Electric Power Systems Research*, Vol. 79, No. 4, pp. 511–520, 2009.

[9] L. T. F. Soares, A. C. D. Souza, W. W. A. G. Silva, L. F. Pugliese, and G. H. Alves, "Grid-Connected Photovoltaic Systems with Energy Storage for Ancillary Services", *Energies*, Vol. 16, No. 21, p. 7379, 2023.

[10] M. Mokhlis, M. Ferfra, and R. Idrissi, "High Gain Observer-Based Control for Grid-Connected PV System Under Partial Shading Effect", *International Journal of Intelligent Engineering and Systems*, Vol. 13, No. 2, pp. 161–172, 2020, doi: 10.22266/ijies2020.0430.16.

[11] E. R. Dalimunthe, E. Susanto, and K. B. Adam, "Improvement of Perturb and Observe Based on Reinforcement Learning for Maximum Power Point Tracking Under Fast Changing Condition", *International Journal of Intelligent Engineering and Systems*, Vol. 16, No. 3, pp. 322–331, 2023, doi: 10.22266/ijies2023.0630.26.

[12] J. Patel, H. Chandwani, V. Patel, and H. Lakhani, "Bi-directional DC-DC converter for battery charging & Discharging applications using buck-boost switch", In: *Proc. of 2012 IEEE Students' Conference on Electrical, Electronics and Computer Science*, Bhopal, India, pp. 1–4, 2012.

[13] H. Han, X. Hou, J. Yang, J. Wu, M. Su, and J. M. Guerrero, "Review of Power Sharing Control Strategies for Islanding Operation of AC Microgrids", *IEEE Transactions on Smart Grid*, Vol. 7, No. 1, pp. 200–215, 2016.

[14] A. Masmoudi, A. Abdelkafi, L. Krichen, and A. S. Saidi, "An experimental approach for improving stability in DC bus voltage of a stand-alone photovoltaic generator", *Energy*, Vol. 257, p. 124797, 2022.

[15] T. Ma, M. H. Cintuglu, and O. A. Mohammed, "Control of a Hybrid AC/DC Microgrid Involving Energy Storage and Pulsed Loads", *IEEE Trans on Ind Applicat*, Vol. 53, No. 1, pp. 567–575, 2017.

[16] A. Borni, T. Abdelkrim, N. Bouarroudj, and A. Bouchakour, "Optimized MPPT Controllers Using GA for Grid Connected Photovoltaic Systems, Comparative study", *Energy Procedia*, Vol. 119, pp. 278–296, 2017.

[17] I. S. Kim, "Robust maximum power point tracker using sliding mode controller for the three-phase grid-connected photovoltaic system", *Solar Energy*, Vol. 81, No. 3, pp. 405–414, 2007.

[18] H. Özbay, S. Öncü, and M. Kesler, "SMC-DPC based active and reactive power control of grid-tied three phase inverter for PV systems", *International Journal of Hydrogen Energy*, Vol. 42, No. 28, pp. 17713–17722, 2017.

[19] V. J. Chin, Z. Salam, and K. Ishaque, "Cell modelling and model parameters estimation techniques for photovoltaic simulator application: A review", *Applied Energy*, Vol. 154, pp. 500–519, 2015.

[20] S. R. Pendem and S. Mikkili, "Modeling, simulation and performance analysis of solar PV array configurations (Series, Series–Parallel and Honey-Comb) to extract maximum power under Partial Shading Conditions", *Energy Reports*, Vol. 4, pp. 274–287, 2018.

[21] S. Naddami, N. Ababssi, and M. Mokhlis, "Nonlinear Control of a Three-Phase, Double-Stage Grid-Tied Photovoltaic System", in: *Proc. of Lecture Notes in Electrical Engineering, Saidia*, Morocco, Vol. 954, pp. 441–449, 2023.

[22] U. Akram, M. Nadarajah, R. Shah, and F. Milano, "A review on rapid responsive energy storage technologies for frequency regulation in modern power systems", *Renewable and Sustainable Energy Reviews*, Vol. 120, p. 109626, 2020.

[23] K. K. Pandey, M. Kumar, A. Kumari, and J. Kumar, "Bidirectional DC-DC Buck-Boost Converter for Battery Energy Storage System and PV Panel", In: *Proc. of Modeling, Simulation and Optimization*, Vol. 206, pp. 681–693, 2021.

[24] W. J. Yang, D. H. Yu, and Y. B. Kim, "Parameter estimation of lithium-ion batteries and noise reduction using an H∞ filter", *Journal of Mechanical Science and Technology*, Vol. 27, No. 1, pp. 247–256, 2013.

[25] S. Naddami and N. Ababssi, "Power quality optimization using a novel backstepping control of a three-phase grid-connected photovoltaic systems", *International Journal of Electrical and Computer Engineering (IJECE)*, Vol. 13, No. 3, p. 2517, 2023.